

Neutrino-driven convection versus advection in core collapse supernovae

T. Foglizzo¹, L. Scheck² and H.-Th. Janka²

¹ Service d’Astrophysique, DSM/DAPNIA, CEA-Saclay,
AIM - Unité Mixte de Recherche CEA - CNRS - Université Paris VII - UMR n 7158

² Max-Planck-Institute für Astrophysik, Karl-Schwarzschild-Str. 1, D-85741 Garching, Germany

Received ; accepted

Abstract. A toy model is analyzed in order to evaluate the linear stability of the gain region immediately behind a stalled accretion shock, after core bounce. This model demonstrates that a negative entropy gradient is not sufficient to warrant linear instability. The stability criterion is governed by the ratio χ of the advection time through the gain region divided by the local timescale of buoyancy. The gain region is linearly stable if $\chi < 3$. The classical convective instability is recovered in the limit $\chi \gg 3$. For $\chi > 3$, perturbations are unstable in a limited range of horizontal wavelengths centered around twice the vertical size H of the gain region. The threshold horizontal wavenumbers k_{\min} and k_{\max} follow simple scaling laws such that $Hk_{\min} \propto 1/\chi$ and $Hk_{\max} \propto \chi$. These scaling laws are understood as the consequence of a vortical-acoustic cycle within the gain region, fed by the Rayleigh-Taylor growth of vorticity perturbations during advection. The stability of short wavelength perturbations is compared to the “ablative stabilization” of accelerated ablation fronts. The convective stability of the $l = 1$ mode in spherical accretion is discussed, in relation with the asymmetric explosion of core collapse supernovae. The advective stabilization of long wavelength perturbations weakens the possible influence of convection alone on a global $l = 1$ mode. Convection may however cooperate efficiently with a global vortical-acoustic cycle extending below the gain radius.

Key words. Accretion – Hydrodynamics – Instabilities – Shock waves – Supernovae

1. Introduction

Convective instabilities may be an important ingredient of the explosion mechanism of core collapse supernovae. Below the neutrinosphere, they can increase the neutrino luminosity, and in the neutrino heating layer they can help pushing the shock farther out. Convection in the supernova core may also be the seed for the large-scale anisotropies seen in many supernovae and supernova remnants and might be linked to the measured high velocities of young pulsars (e.g., Arnett 1987, Woosley 1987, Herant et al. 1992). Negative gradients of entropy were initially thought to arise as a natural consequence of the decline of the shock strength due to photodissociation of heavy nuclei and neutrino escape (Arnett 1987, Burrows 1987, Bethe, Brown & Cooperstein 1987, Bethe 1990). A more durable effect was recognized by Herant, Benz & Colgate (1992) in their simulations: neutrino heating is able to maintain a negative entropy gradient in a “gain region” immediately behind the stalled shock. They also observed that the convective eddies tend to merge and produce eddies of the size of the computing box. Similar results were found in the numerical simulations of Herant et al. (1994), Burrows et al. (1995), Janka & Müller (1996), Mezzacappa et al. (1998).

Are such convective instabilities able to produce an $l = 1$ asymmetry as suggested by Herant (1995) and Thompson (2000) and seen more recently in numerical simulations (Blondin et al. 2003, Scheck et al. 2004)? Estimates of the linear growth rate and wavelength of the nonspherical modes found in these studies cannot be directly made on grounds of the considerations of convective instabilities in hydrostatic spherical shells (e.g., Chandrasekar 1961). Attention has to be paid to the fact that the advection of matter across the shock and through the gain region might seriously reduce the convective growth rate and modify the spatial structure of unstable modes.

The nonspherical modes of deformation of an accretion shock discovered in adiabatic numerical simulations by Blondin et al. (2003), which the authors termed SASI—standing accretion shock instability—suggest the importance of another instability, independent of convection, in the core collapse problem. Below we will argue that the underlying mechanism is an advective-acoustic instability, which is based on the acoustic feedback produced by the advection of entropy and vorticity perturbations from the shock to the accretor (Foglizzo & Tagger 2000, Foglizzo 2001, 2002). More realistic simulations by Scheck et al. (2004), including neutrino heating, a microphysical equation of state and the environment of collapsing stellar cores, recognized the development of a strong

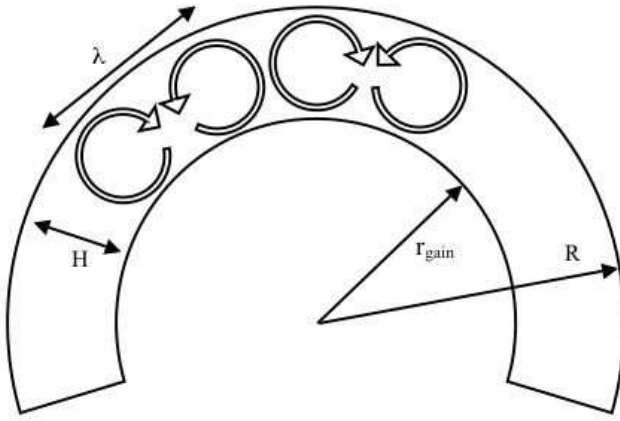


Fig. 1. Schematic view of convection in a spherical shell of size H . The first unstable modes when viscosity is decreased have a wavelength $\lambda \sim (2-3)H$, depending on the boundary conditions (Chandrasekhar 1961)

$l = 1$ mode possibly due to the combination of convective and advective-acoustic instabilities. The asymmetry produced by this instability makes it a good candidate to explain the high velocities of pulsars.

Is it possible to disentangle the convective and the advective-acoustic instabilities from the point of view of their linear growth rates and spatial structure? As a first step, this study aims at a better characterization of neutrino-driven convection in the gain layer beyond the classical hydrostatic approach. The effects of any acoustic feedback produced *below* the gain radius are thus neglected in the present analysis. The classical results for the convective instability in plane and spherical geometry are recalled in Sect. 2. A simple toy model incorporating the minimum ingredients leading to the convective instability below a stationary shock is described in Sect. 3. The stabilization of the convective mode by advection is studied in Sect. 4 by solving numerically the eigenvalue problem. In Sect. 5, the mechanism of stabilization is discussed and compared to known results in accelerated ablation fronts. These results obtained in planar geometry are extrapolated to spherical geometry in Sect. 6, in order to discuss the convective stability of the mode $l = 1$. In Sect. 7 we will summarize our findings and draw conclusions.

2. Classical results about the onset of convection in a hydrostatic equilibrium

In the absence of viscosity and of stabilizing composition gradients, a stratified atmosphere with a negative entropy gradient is unstable at all wavelengths. Perturbations with a horizontal wavelength shorter than the scale height H of the entropy gradient are the most unstable. A measure of the entropy is defined by the dimensionless quantity S , as a function of pressure P and density ρ :

$$S \equiv \frac{1}{\gamma - 1} \log \left[\frac{P}{P_{\text{sh}}} \left(\frac{\rho_{\text{sh}}}{\rho} \right)^{\gamma} \right]. \quad (1)$$

The maximum growth rate ω_{buoy} is given by the Brunt-Väisälä frequency, expressed by the gravitational acceleration G and H :

$$\omega_{\text{buoy}} \equiv G^{\frac{1}{2}} \left| \frac{\nabla P}{\gamma P} - \frac{\nabla \rho}{\rho} \right|^{\frac{1}{2}} = \left(\frac{\gamma - 1}{\gamma} G \nabla S \right)^{\frac{1}{2}} \sim \left(\frac{G}{H} \right)^{\frac{1}{2}}. \quad (2)$$

Perturbations with a longer horizontal wavelength than H are also unstable, with a slower growth rate however. Perturbations with a horizontal wavelength much shorter than H are easily stabilized by a small amount of viscosity. This is illustrated by the calculations of Chandrasekhar (1961) of the onset of convection, either between two parallel plates or in a spherical shell. These calculations measured the amount of viscosity which is required to stabilize a perturbation with a given wavelength. The wavelength of the first unstable mode is about $[2 - 3]$ times the vertical size of the unstable region depending on the nature of the boundaries (free, rigid or mixed). Note that a factor 2 would be rather intuitive, since it corresponds to a pair of two counter-rotating circular eddies (see Fig. 1). In a spherical shell, a naive estimate of the azimuthal number l of the first unstable perturbations, based on the number of pairs of circular eddies which would fit in the unstable shell $r_{\text{gain}} < r < R$, leads to:

$$l \sim \frac{\pi}{2} \frac{R + r_{\text{gain}}}{H}. \quad (3)$$

This simplistic approach is compatible with the exact calculations performed by Chandrasekhar (1961), within the same factor $1 - 2$ as in the case of Benard convection (Rayleigh 1916). This factor depends on the boundary conditions, on the gravity profile, and can be interpreted as an aspect ratio of the eddies, which are not circular. A direct application to the size of a stalled shock with $R \sim 150$ km and $r_{\text{gain}} \sim 100$ km, as in Herant, Benz & Colgate (1992), would lead to $l \sim 7$. As noted by Herant, Benz & Colgate (1992), the increase of H naturally leads to the decrease of the optimal l . Is the residual instability of the $l = 1$ mode fast enough to have a significant influence during the first second after core bounce? The classical description by Chandrasekhar is not directly applicable here, not only because viscosity is negligible, but also because it does not take into account the presence of a shock wave, and the associated flow of gas across it. Let us compare the timescale of buoyancy $\omega_{\text{buoy}}^{-1}$ with the advection timescale H/v_{sh} through the gain region. In what follows, the subscript “1” refers to preshock quantities, and the subscript “sh” is used for postshock quantities immediately after the shock. The local gravity at the shock radius r_{sh} is $G \equiv GM/r_{\text{sh}}^2$. Assuming that the gas is in free fall ahead of the shock ($v_1^2 \sim 2GM/r_{\text{sh}}$), one estimates:

$$\frac{H\omega_{\text{buoy}}}{v_{\text{sh}}} \sim \left(\frac{GM}{r_{\text{sh}} v_{\text{sh}}^2} \right)^{\frac{1}{2}} \left(\frac{H}{r_{\text{sh}}} \right)^{\frac{1}{2}} \sim \left(\frac{v_1}{v_{\text{sh}}} \right) \left(\frac{H}{2r_{\text{sh}}} \right)^{\frac{1}{2}}, \quad (4)$$

$$\sim 3.1 \left(\frac{v_1}{7v_{\text{sh}}} \right) \left(\frac{H}{0.4r_{\text{sh}}} \right)^{\frac{1}{2}}. \quad (5)$$

A typical radius of the stalled shock is $r_{\text{sh}} \sim 150$ km, and $0.3 \leq H/r_{\text{sh}} \leq 0.5$. The velocity jump across the shock would be $v_1/v_{\text{sh}} = 7$ for an adiabatic gas with $\gamma = 4/3$. This ratio may increase up to $v_1/v_{\text{sh}} \sim 10$ due to dissociation of iron into nucleons. Even then, the rough estimate of Eq. (5) indicates that

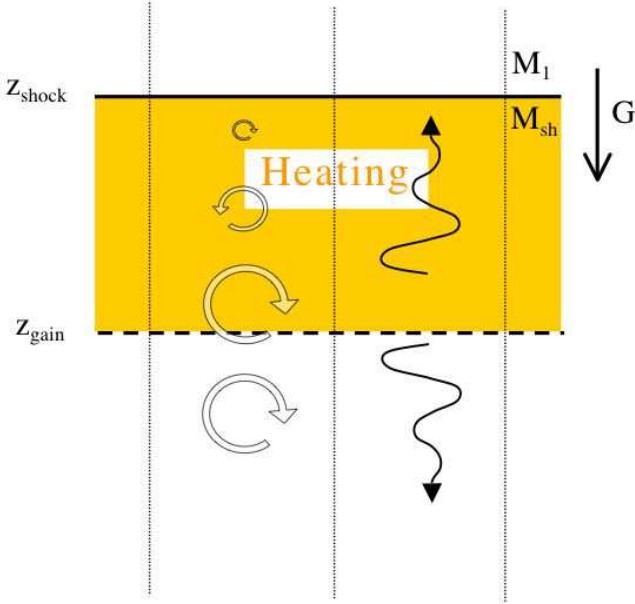


Fig. 2. Schematic view of the toy model enabling the convective instability in the gain region immediately below a shock. The entropy gradient is oriented downward in the gain region. Entropy/vorticity perturbations (circular arrows) are advected downward with the flow, and can be coupled to acoustic ones (wavy arrows) at low frequency.

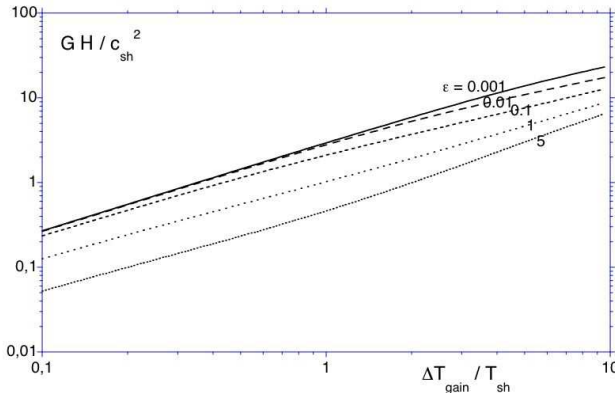


Fig. 3. Size H of the gain region, in units of c_{sh}^2/G , function of the parameters ϵ and $\Delta T_{\text{gain}}/T_{\text{sh}}$. The shock is adiabatic ($\mathcal{M}_1 = 5$ in all plots).

the convective growth time is comparable to the advection time through the gain region.

3. Description of a planar toy model

3.1. Stationary flow

This 1-D toy model mimics the accretion flow in the gain region immediately below the stalled accretion shock, a few tens of milliseconds after core bounce. The flow is described by a

perfect gas with an adiabatic index $\gamma = 4/3$, corresponding to a gas of relativistic electrons or photons and electron-positron pairs. We shall further assume that $P \propto \rho T$ (with T being the temperature), which is a suitable description of the thermodynamic conditions in the gain layer independent of whether relativistic particles or baryons dominate the pressure (for details, see Janka 2001, Bethe 1993).

3.1.1. Photodissociation at the shock

The effect of dissociation can be crudely incorporated by assuming that it takes place immediately behind the shock. It is parametrized in Appendix A by a decrease of the postshock Mach number \mathcal{M}_{sh} below the adiabatic value \mathcal{M}_{ad} :

$$\mathcal{M}_{\text{sh}} \leq \mathcal{M}_{\text{ad}} \equiv \left[\frac{2 + (\gamma - 1)\mathcal{M}_1^2}{2\gamma\mathcal{M}_1^2 - \gamma + 1} \right]^{\frac{1}{2}}. \quad (6)$$

In the phase of a stalled accretion shock the gravitating mass is $M \sim 1.2 M_{\odot}$ and the preshock sound speed is $c_1 \sim 8.5 \times 10^8 \text{ cm s}^{-1}$. The incident Mach number \mathcal{M}_1 is estimated assuming free-fall velocity of the gas incident at the shock:

$$|v_1| \sim \left(\frac{2GM}{r_{\text{sh}}} \right)^{\frac{1}{2}} \sim 4.6 \left(\frac{r_{\text{sh}}}{150 \text{ km}} \right)^{-\frac{1}{2}} \times 10^9 \text{ cm s}^{-1}, \quad (7)$$

$$\mathcal{M}_1 \sim 5.4 \left(\frac{r_{\text{sh}}}{150 \text{ km}} \right)^{-\frac{1}{2}}. \quad (8)$$

The incident Mach number is taken equal to $\mathcal{M}_1 = 5$ in the rest of the paper, so that $\mathcal{M}_{\text{ad}} \sim 0.39$. A prescription $\mathcal{M}_{\text{sh}}/\mathcal{M}_{\text{ad}} = 0.77$ accounting for dissociation corresponds to more realistic values of $\mathcal{M}_{\text{sh}} \sim 0.3$, a velocity jump $v_1/v_{\text{sh}} \sim 8.8$ and a jump of sound speed $c_{\text{sh}}/c_1 \sim 1.85$. Dissociation at the shock also plays the role of an additional parameter of our toy model, influencing directly the advection time within the gain region. Considering the full range $1/(\gamma\mathcal{M}_1) < \mathcal{M}_{\text{sh}} \leq \mathcal{M}_{\text{ad}}$ allows us to explore the stability of a larger family of flows, and thus better understand the onset of convection. The extreme case $\mathcal{M}_{\text{sh}}\mathcal{M}_1 = 1/\gamma$ corresponds to $c_{\text{sh}} = c_1$ and $v_1/v_{\text{sh}} = \gamma\mathcal{M}_1^2$ is referred to as the “isenthalpic shock”.

3.1.2. Gain region

The essential ingredients of the convective instability are the entropy changes and the local acceleration. In the present model, the local acceleration is mainly due to a uniform gravity G . The entropy gradient ∇S is produced by the heating through neutrino absorption, which exceeds the cooling by neutrino emission in the gain region $z_{\text{gain}} < z < z_{\text{sh}}$. $H \equiv z_{\text{sh}} - z_{\text{gain}}$ is the size of the gain region. The heating/cooling function is adapted from Bethe & Wilson (1985), neglecting the effect of geometric dilution of the neutrino flux:

$$\mathcal{L} \equiv \frac{\bar{\mathcal{L}}\rho}{1 - \beta} \left[1 - \beta \left(\frac{T}{T_{\text{sh}}} \right)^6 \right], \quad (9)$$

$$\bar{\mathcal{L}} \sim 2.2 \left(\frac{r_{\text{sh}}}{150 \text{ km}} \right)^{-2} \times 10^{20} \text{ ergs g}^{-1} \text{ s}^{-1}, \quad (10)$$

where T_{sh} is the postshock temperature. $\beta < 1$ is defined as the ratio of the strengths of neutrino cooling and neutrino heating

at the shock. The gain radius r_{gain} is defined as the point where $\mathcal{L} = 0$. According to Eq. (9), the temperature at the gain radius is $T_{\text{gain}} = T_{\text{sh}}/\beta^{\frac{1}{6}}$. Cooling and heating are neglected above the shock, and also below the gain radius. Convergence of the flow and self-gravity are neglected, too. Using the definition (1) of S and the relation $c^2 \equiv \gamma P/\rho$, the pressure force is expressed as follows:

$$\frac{\nabla P}{\rho} = \nabla \left(\frac{c^2}{\gamma - 1} \right) - \frac{c^2}{\gamma} \nabla S. \quad (11)$$

The equation of continuity, the Euler equation and the entropy equation defining the stationary flow in the gain region are:

$$\frac{\partial}{\partial z}(\rho v) = 0, \quad (12)$$

$$\frac{\partial}{\partial z} \left(\frac{v^2}{2} + \frac{c^2}{\gamma - 1} + Gz \right) = \frac{\mathcal{L}}{\rho v}, \quad (13)$$

$$\frac{\partial S}{\partial z} = \frac{\mathcal{L}}{Pv}, \quad (14)$$

where the last relation makes use of $P \propto \rho T$. The local acceleration of the flow $\partial v/\partial z$, deduced from these equations, contains two opposite contributions from gravity and heating:

$$\frac{1}{v} \frac{\partial v}{\partial z} = \frac{1}{c^2 - v^2} \left[G + (\gamma - 1) \frac{\mathcal{L}}{\rho v} \right]. \quad (15)$$

The heating constant $\bar{\mathcal{L}} > 0$ is normalized by the amount of heating needed to cancel the acceleration of the gas immediately behind the shock, as deduced from Eq. (15):

$$\epsilon \equiv -(\gamma - 1) \frac{\bar{\mathcal{L}}}{Gv_{\text{sh}}} > 0. \quad (16)$$

The vertical derivative of S is expressed using its value ∇S_{sh} at the shock, rewritten in our dimensionless units:

$$\nabla S_{\text{sh}} = -\frac{\gamma \epsilon}{\gamma - 1} \frac{G}{c_{\text{sh}}^2}, \quad (17)$$

$$\frac{\partial S}{\partial z} = \frac{v_{\text{sh}}}{v} \frac{c_{\text{sh}}^2}{c^2} \frac{\nabla S_{\text{sh}}}{1 - \beta} \left[1 - \beta \left(\frac{T}{T_{\text{sh}}} \right)^6 \right]. \quad (18)$$

In addition to $\gamma \sim 4/3$ and $\mathcal{M}_1 \sim 5$, the independent parameters of this toy model are the dissociation parameter $\mathcal{M}_{\text{sh}}/\mathcal{M}_{\text{ad}}$, and two parameters $T_{\text{sh}}/T_{\text{gain}}$, ϵ describing the strength of gravity and heating. Denoting by $\Delta T_{\text{gain}} \equiv T_{\text{gain}} - T_{\text{sh}}$ the temperature increase in the gain region, the interdependence of ϵ , $\Delta T_{\text{gain}}/T_{\text{sh}}$ and GH/c_{sh}^2 in this toy model is visualized in Fig. 3 for a flow without dissociation. In our dimensionless units, the intensity of heating is:

$$\epsilon \sim 0.16 \left(\frac{v_1}{7v_{\text{sh}}} \right) \left(\frac{r_{\text{sh}}}{150 \text{ km}} \right)^{\frac{1}{2}}. \quad (19)$$

3.2. Existing results about radial stability

According to the linear stability analysis of Yamasaki & Yamada (2005), the stationary flow described by Burrows & Goshy (1993) is always stable with respect to radial perturbations. The flow is neutrally stable at best, when parameters

reach the boundary of the domain of existence of a stationary solution. They also found that another shock position (further out), where the post-shock Mach number increases inward, is radially unstable.

In our toy model, the Mach number always decreases inward behind the shock for $\epsilon \leq 1$ (see Appendix F.1). The flow described by our toy model is thus expected to be stable with respect to radial perturbations. It remains to be explored whether a radial instability occurs at a certain threshold $\epsilon > 1$.

Note that even if heating were sufficiently strong to make the flow accelerate inward immediately behind the shock ($\partial v^2/\partial z < 0$, i.e. $\epsilon > 1$), the vertical gradient of the total pressure $P + \rho v^2$ would still increase outward across the shock (see Appendix F.1). The heuristic physical argument of Nobuta & Hanawa (1994) about the reacceleration instability (Nakayama 1992, Foglizzo 2002) therefore also leads us to expect radial stability, if the shock is strong enough.

3.3. Linear perturbations

3.3.1. Differential system

The 1-D stationary flow is perturbed in the plane x, z . The linearized equations are described in Appendix B as a differential system of fourth order. The natural functions of the perturbative approach are f , h , δS and δK , with

$$f \equiv v \delta v + \frac{2}{\gamma - 1} c \delta c, \quad (20)$$

$$h \equiv \frac{\delta v}{v} + \frac{\delta \rho}{\rho}, \quad (21)$$

$$\delta K \equiv i v k_x \delta w_y + \frac{k_x^2 c^2}{\gamma} \delta S, \quad (22)$$

where k_x is the horizontal wavenumber and δw_y is the perturbation of vorticity. In the adiabatic limit, the perturbations δS and δK are conserved when advected (Foglizzo 2001, hereafter F01). If $\omega \neq 0$,

$$\frac{\partial f}{\partial z} = \frac{i \omega v}{1 - \mathcal{M}^2} \left\{ h - \frac{f}{c^2} + \left[\gamma - 1 + \frac{1}{\mathcal{M}^2} \right] \frac{\delta S}{\gamma} \right\} + \delta \left(\frac{\mathcal{L}}{\rho v} \right), \quad (23)$$

$$\frac{\partial h}{\partial z} = \frac{i \omega}{v(1 - \mathcal{M}^2)} \left\{ \frac{\mu^2}{c^2} f - \mathcal{M}^2 h - \delta S \right\} + \frac{i \delta K}{\omega v}, \quad (24)$$

$$\frac{\partial \delta S}{\partial z} = \frac{i \omega}{v} \delta S + \delta \left(\frac{\mathcal{L}}{\rho v} \right), \quad (25)$$

$$\frac{\partial \delta K}{\partial z} = \frac{i \omega}{v} \delta K + k_x^2 \delta \left(\frac{\mathcal{L}}{\rho v} \right), \quad (26)$$

where \mathcal{L} is the heating/cooling function and μ is defined by:

$$\mu^2 \equiv 1 - \frac{k_x^2 c^2}{\omega^2} (1 - \mathcal{M}^2). \quad (27)$$

μ is a natural parameter in the algebraic formulation of the problem. When the frequency ω is real, μ is directly related to the angle ψ between the direction of propagation of the wave and the direction of the flow. Correcting a typing error in Eq. (E11) of F02:

$$\tan^2 \psi = \frac{1 - \mu^2}{\mu^2 (1 - \mathcal{M}^2)}. \quad (28)$$

3.3.2. Boundary condition at the shock

The boundary conditions at the shock surface are obtained using conservation laws in the frame of the perturbed shock:

$$f_{\text{sh}} = \Delta v(v_{\text{sh}} - v_1) - \Delta \zeta \frac{c^2}{\gamma} \nabla S_{\text{sh}}, \quad (29)$$

$$h_{\text{sh}} = \frac{\Delta v}{v_{\text{sh}}} \left(1 - \frac{v_{\text{sh}}}{v_1} \right), \quad (30)$$

$$\frac{\delta S_{\text{sh}}}{\gamma} = -\Delta \zeta \left[\frac{\nabla S_{\text{sh}}}{\gamma} + \left(1 - \frac{v_{\text{sh}}}{v_1} \right) \frac{G}{c^2} \right] - \frac{v_1 \Delta v}{c^2} \left(1 - \frac{v_{\text{sh}}}{v_1} \right)^2, \quad (31)$$

$$\delta K_{\text{sh}} = -k_x^2 \Delta \zeta \frac{c^2}{\gamma} \nabla S_{\text{sh}}, \quad (32)$$

where the velocity of the shock is related to its displacement through $\Delta v \equiv -i\omega \Delta \zeta$. In these equations, the cooling/heating above the shock is neglected ($\mathcal{L}_1 \ll \mathcal{L}_{\text{sh}}$). The vorticity $\delta \omega_y$ produced by the perturbed shock, deduced from Eqs. (F.4), (31) and (32), is independent of heating:

$$(\delta \omega_y)_{\text{sh}} = -\frac{ik_x}{v_{\text{sh}}} \left(1 - \frac{v_{\text{sh}}}{v_1} \right) [(v_1 - v_{\text{sh}}) \Delta v + G \Delta \zeta]. \quad (33)$$

These boundary conditions agree with FGR05 when heating is suppressed.

3.3.3. Leaking condition at the lower boundary

The effect of negative entropy gradients within the gain region are separated from any coupling process below the gain radius by choosing a leaking boundary condition at the gain radius:

- entropy and vorticity perturbations reaching the gain radius are simply advected downward,

- acoustic perturbations are free to propagate downward, with no reflexion.

This boundary condition is equivalent to replacing the accretion flow below the gain radius by a uniform flow. The uniformity of the flow warrants the absence of coupling processes. Each perturbation is decomposed in Appendix C as the sum of entropy, vorticity, and pressure perturbations:

$$f = f_S + f_K + f_+ + f_-, \quad (34)$$

$$h = h_S + h_K + h_+ + h_-. \quad (35)$$

The absence of coupling below the gain radius corresponds to the absence of an acoustic flux from below ($f_- = 0, h_- = 0$):

$$\frac{\mu}{\mathcal{M}} \frac{f}{c^2} - h - \left(\gamma + \frac{\mu}{\mathcal{M}} \frac{1 - \mathcal{M}^2}{1 + \mu \mathcal{M}} \right) \frac{\delta S}{\gamma} + \frac{1 - \mu^2}{1 + \mu \mathcal{M}} \frac{\delta K}{k_x^2 c^2} = 0. \quad (36)$$

4. Convective mode in the gain region

4.1. Definition of the ratio χ comparing the advective and buoyancy timescales

The maximum growth rate ω_{buoy} of the convective instability (Eq. 2) can be expressed with the local variables ϵ, T, v, c as a function of height z :

$$\omega_{\text{buoy}}(z) = \epsilon^{\frac{1}{2}} \left| \frac{v_{\text{sh}}}{v} \right|^{\frac{1}{2}} \left[\frac{1 - (T/T_{\text{gain}})^6}{1 - (T_{\text{sh}}/T_{\text{gain}})^6} \right]^{\frac{1}{2}} \frac{G}{c}, \quad (37)$$

$$\omega_{\text{max}} \equiv \text{Max}_{z_{\text{gain}} < z < z_{\text{sh}}} \omega_{\text{buoy}}(z). \quad (38)$$

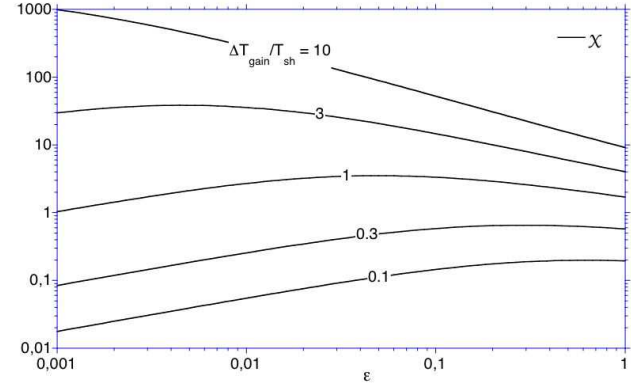


Fig. 4. Ratio χ of the advective and convective timescales in our toy model with an adiabatic shock, as function of the heating parameter ϵ , for different values of $\Delta T_{\text{gain}}/T_{\text{sh}}$ indicated on each curve.

Note that $\epsilon^{\frac{1}{2}}$ directly measures the growth rate of the convective instability at the shock, in units of G/c_{sh} :

$$\omega_{\text{buoy}}^{\text{sh}} = \epsilon^{\frac{1}{2}} \frac{G}{c_{\text{sh}}}. \quad (39)$$

When considered as a local instability, the transient amplification of short wavelength perturbations, during their advection through the gain region, can be estimated by the quantity $\exp \chi$, with

$$\chi \equiv \int_{\text{gain}}^{\text{shock}} \omega_{\text{buoy}}(z) \frac{dz}{v}. \quad (40)$$

The correspondence between $\epsilon, \Delta T_{\text{gain}}/T_{\text{sh}}$ and χ is shown in Fig. 4. Approximating the entropy gradient $\nabla S \sim \Delta S/H$, χ can be compared to the Froude number Fr defined as the ratio of the kinetic and gravitational energies in the gain region:

$$\chi \sim \left(\frac{G \Delta S}{H} \right)^{\frac{1}{2}} \frac{H}{v} \sim \left(\frac{G H}{v^2} \right)^{\frac{1}{2}} (\Delta S)^{\frac{1}{2}} \propto \text{Fr}^{-\frac{1}{2}}. \quad (41)$$

4.2. Numerical solution of the eigenmode problem

The numerical solution of the boundary value problem reveals that a global unstable mode grows exponentially with time if the advection timescale is long enough compared to the convective timescale. The existence of a global convective mode appears to depend directly on whether the ratio χ , defined by Eq. (40), is above or below a certain threshold χ_0 .

As an illustration, Fig. 5 shows the effect of advection on the convective instability for $\epsilon = 0.1$, where $1 \leq \Delta T_{\text{gain}}/T_{\text{sh}} \leq 10$ is varied so that $3 < \chi < 53$. The convective growth is measured in units of ω_{max} , and the wavenumber in units of H . The classical convective instability is recovered in the limit $\chi \gg 1$. The effects of advection can be summarized as follows:

(i) The growth rate is decreased compared to the maximum value of the local convective growth rate ω_{max} (Eq. (38)),

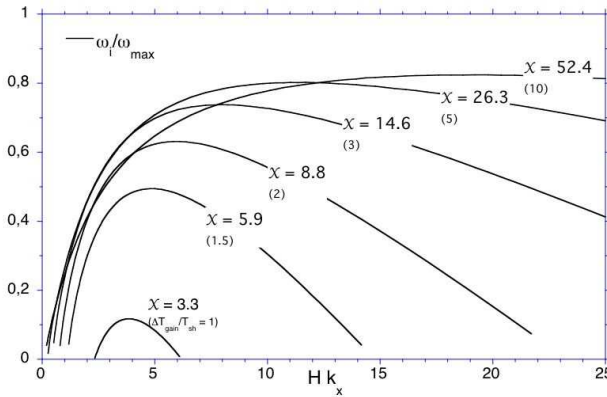


Fig. 5. Growth rate of the convective instability as a function of the horizontal wavenumber. Growth rates are normalized to ω_{\max} . Heating is such that $\epsilon = 0.1$. The shock is adiabatic. The ratio χ of the advective and convective timescales is indicated on each curve, with the corresponding temperature contrast $\Delta T_{\text{gain}}/T_{\text{sh}}$ given in parentheses. Advection stabilizes both the long and short wavelengths. The convective instability disappears for $\chi < 3$.

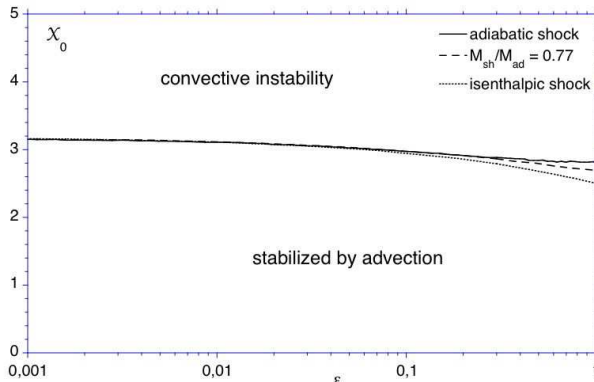


Fig. 6. Threshold χ_0 of the ratio of the convective and advective timescales, determining the existence of the convective mode, as a function of the intensity ϵ of heating. This threshold is essentially insensitive to dissociation at the shock.

- (ii) short wavelength perturbations are stable,
- (iii) long wavelength perturbations are also stable.

In Fig. 5, the convective instability disappears completely for $\chi \leq 3$. The flow is then stable although the entropy gradient is negative. Even when the heating coefficient ϵ is varied over three orders of magnitude, the threshold of marginal stability always corresponds to $\chi \sim 3$, as shown in Fig. 6 for an adiabatic shock (full line). This threshold is approximately insensitive to the loss of energy at the shock (dashed and dotted lines). The stability threshold in Fig. 6 and in subsequent figures is obtained by solving the boundary value problem correspond-

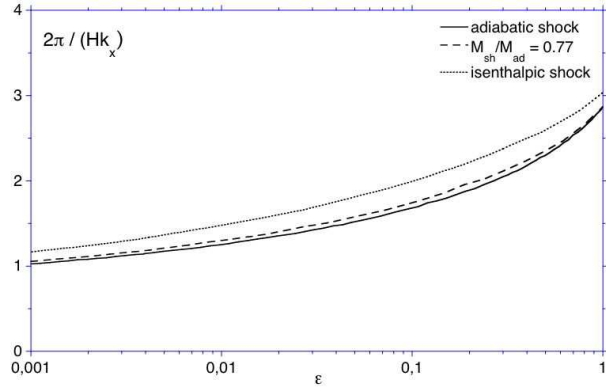


Fig. 7. Wavelength of the neutral mode corresponding to the threshold value χ_0 , in units of the size of the gain region.

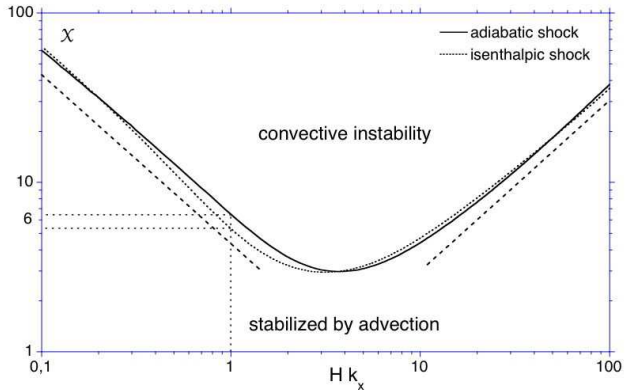


Fig. 8. Range of horizontal wavenumbers allowing the convective instability, for $\epsilon = 0.1$, when the ratio χ is varied as in Fig. 5. The slopes ± 1 are indicated as dotted lines for comparison.

ing to the neutral mode (i.e. $\omega = 0$), as shown in Appendix D. According to Fig. 7, the wavelength of the neutral mode for $\chi = \chi_0$ is comparable to $[1 - 3]$ times the size H of the gain region, with very little influence of dissociation at the shock. A similar range was obtained for the first unstable mode in classical convection stabilized by viscosity (Sect. 2).

The range of unstable wavenumbers decreases with χ in a very simple way illustrated by Fig. 8 for $\epsilon = 0.1$. When measured in units of $1/H$, the minimal and maximal wavenumbers are proportional to χ^{-1} and χ respectively.

5. Discussion of the mechanism of stabilization

The existence of a stability threshold measured by χ can be interpreted in terms of energy. According to Eq. (41), χ^2 is also a measure of the potential energy in the gain region divided by the kinetic energy. The convective instability is indeed driven

by the potential energy, which is liberated by the interchange of high entropy and low entropy gas. The global instability requires that the energy gained from the interchange is large enough to overcome the kinetic energy of the gas. This interpretation is qualitative and does not explain, in particular, the numerical value ($\chi_0 \sim 3$) of the threshold.

5.1. Stabilization of short wavelengths: a vortical-acoustic cycle fed by buoyancy, within the gain region

The simple scaling measured numerically in Fig. 8 calls for a simple physical mechanism. A tentative explanation of the stabilization mechanism follows the ideas developed for the advective-acoustic instabilities. As recalled in Foglizzo, Galletti & Ruffert (2005), in the most general form advective-acoustic cycles consist of four phases: advection of entropy/vorticity perturbations, coupling to pressure perturbations, propagation of pressure perturbations, coupling to advected perturbations.

In a reference frame moving with the flow from z_{sh} to z_0 , the acceleration and entropy gradients are such that vorticity perturbations are Rayleigh-Taylor unstable. A vorticity perturbation δw with a short wavelength $Hk_x \gg 1$ should grow like

$$\delta w \propto \exp \left(\int_{z_{\text{sh}}}^{z_0} \omega_{\text{buoy}}(z) \frac{dz}{v} \right), \quad (42)$$

where $\omega_{\text{buoy}}(z)$ is the local growth rate of the Rayleigh-Taylor instability in the moving fluid. If vorticity were decoupled from pressure, this growth would cease when the advected perturbation reaches the gain radius, and the flow would be globally stable. Vorticity and pressure are actually coupled by the flow gradients in the gain region, and particularly by the sudden drop of the buoyant growth rate at the gain radius (Fig. 9). Let us assume that most of the coupling takes place at the height z_{∇} close to the gain radius, with an efficiency Q_{∇} :

$$\delta p \propto Q_{\nabla} \delta w. \quad (43)$$

A pressure perturbation with a horizontal wavelength $2\pi/k_x$ shorter than the vertical scale H of the flow gradients, localized at a height z_{∇} , produces a hydrostatic pressure perturbation in the vertical direction. At a distance $|z - z_{\nabla}|$ below or above it, this pressure perturbation decays exponentially like

$$\delta p \propto \exp(-k_x|z - z_{\nabla}|), \quad (44)$$

$$\propto \exp \left(- \left| \int_{z_{\nabla}}^z k_x v \frac{dz}{v} \right| \right). \quad (45)$$

Conversely, pressure perturbations are coupled to vorticity perturbations through the shock, with an efficiency Q_{sh} :

$$\delta w \propto Q_{\text{sh}} \delta p \quad (46)$$

The global efficiency Q of this vortical-acoustic cycle is:

$$Q \equiv Q_{\nabla} Q_{\text{sh}} \exp \left[\int_{z_{\text{sh}}}^{z_{\nabla}} (\omega_{\text{buoy}} - k_x v) \frac{dz}{v} \right]. \quad (47)$$

A necessary condition for the instability of this vortical-acoustic cycle is that the local rate of exponential increase ω_{buoy}

is fast enough to overcome both the evanescent pressure feedback and the possibly modest coupling efficiencies $|Q_{\nabla} Q_{\text{sh}}|$. Let us denote by (ω_r, ω_i) the real and imaginary parts of the eigenfrequency ω . If the purely acoustic cycle is negligible and $|Q| > 1$, the growth rate ω_i is approximately:

$$\omega_i \sim \frac{1}{\tau_Q} \log Q, \quad (48)$$

where τ_Q is the duration of the advective-acoustic cycle.

The accretion flow studied in F02 exhibited overstable modes, fed by strong coupling constants $|Q_{\nabla}| \gg 1$ if $\gamma \sim 5/3$ (FT00, F01) or $|Q_{\text{sh}}| \gg 1$ if $\gamma \sim 1$ (F02). In these examples, the lowest oscillation frequency ω_r was of the order of $2\pi/\tau_Q$, in the pseudosound domain. The present case of neutrino-driven convection is an example of an unstable cycle where neither $|Q_{\nabla}|$ nor $|Q_{\text{sh}}|$ are large, but where the increase of vorticity during advection compensates for the evanescence of the pressure feedback. A purely growing mode may exist (i.e. $\omega_r = 0$) if Q is real, and $Q > 1$. Using Eq. (47), this condition becomes:

$$\int_{z_{\text{sh}}}^{z_{\nabla}} (\omega_{\text{buoy}} - k_x v) \frac{dz}{v} + \log Q_{\nabla} Q_{\text{sh}} > 0. \quad (49)$$

According to the definition of χ , and approximating $|z_{\text{sh}} - z_{\nabla}| \sim H$, the condition (49) translates into:

$$Hk_x < \chi + \log Q_{\nabla} Q_{\text{sh}}. \quad (50)$$

Strictly speaking, the coupling coefficients Q_{∇} and Q_{sh} depend on k_x . The function $Q_{\text{sh}}(k_x)$ can be deduced explicitly from the conservation equations at the shock, as was done in FT00, F02 and FGR05. $Q_{\text{sh}}(k_x)$ is an algebraic function of k_x . Assuming that the k_x dependence of Q_{∇} is also algebraic, the maximum wavenumber k_{max} when $\chi \gg 1$ is asymptotically governed by χ :

$$Hk_{\text{max}} \propto \chi \propto F^{-\frac{1}{2}}. \quad (51)$$

The asymptotic behaviour $Hk_{\text{max}} \propto \chi$ observed in Fig. 8 is thus interpreted as the threshold where the local convective instability compensates for the evanescent pressure feedback.

5.2. Long wavelength stabilization of convection

The stabilization of long wavelength perturbations seen in Fig. 8 can be deduced by an extrapolation of the preceding formalism at long horizontal wavelengths. We show in Appendix D that the growth rate of the Rayleigh-Taylor instability in a smoothly stratified fluid at rest, close to a fixed boundary (either rigid or free), is proportional to k_x for long wavelength perturbations ($Hk_x \ll 1$). A global formula can be approximated by

$$\omega_{\text{buoy}}(k_x) \sim \frac{Hk_x}{(H^2 k_x^2 + \zeta^2)^{\frac{1}{2}}} \omega_{\text{buoy}}, \quad (52)$$

where $\omega_{\text{buoy}} \sim (G/H)^{1/2}$ is the short wavelength growth rate. The value $1/2 \leq \zeta \leq 5$ depends mainly on the specific profile of the stratification, and marginally on the value of k_x . The pressure feedback for very long wavelength perturbations $Hk_x \ll 1$

scales like $\exp[-(z - z_\nabla)/H]$ rather than Eq. (44). The extrapolation for long wavelength perturbations of Eqs. (47) and (50) are thus:

$$Q \equiv Q_\nabla Q_{\text{sh}} \exp \left[\int_{z_{\text{sh}}}^{z_\nabla} \left(\frac{Hk_x}{\zeta} \omega_{\text{buoy}} - \frac{v}{H} \right) \frac{dz}{v} \right], \quad (53)$$

$$\frac{Hk_x}{\zeta} \chi > 1 - \log Q_\nabla Q_{\text{sh}}. \quad (54)$$

Assuming again an algebraic k_x -dependence of the coupling efficiencies, for $Hk_x \ll 1$, the minimum wavenumber k_{\min} satisfying Eq. (54) for $\chi \gg 1$ sets a lower bound on the ratio of the advection timescale H/v and the local convective growth time $1/\omega_{\text{buoy}}(k_x)$:

$$Hk_{\min} \propto \chi^{-1} \propto \text{Fr}^{\frac{1}{2}}. \quad (55)$$

The slope $Hk_{\min} \propto \chi^{-1}$ observed in Fig. 8 is thus interpreted as a direct consequence of the relation $\omega_{\text{buoy}} \propto k_x$ close to a boundary. A similar effect was present in Problem 2 of Chapt. 12 in Landau & Lifschitz (1989), where the growth rate of the Rayleigh-Taylor instability is $\propto k_x$ if a boundary stands at a distance shorter than k_x^{-1} from a density step.

5.3. Estimate of the maximum convective growth rate with advection

If $|Q| \gg 1$, the growth rate ω_i deduced from Eq. (48) is

$$\omega_i \sim \frac{1}{\tau_Q} \left\{ \int_{z_{\text{sh}}}^{z_\nabla} (\omega_{\text{buoy}}(z, k_x) - k_x v) \frac{dz}{v} + \log Q_\nabla Q_{\text{sh}} \right\}, \quad (56)$$

The cycle timescale τ_Q includes the acoustic timescale τ_- of the pressure feedback. The integrals can be rewritten by introducing a specific height z_i and z_j such that:

$$\tau_Q \equiv \int_{z_{\text{sh}}}^{z_\nabla} \frac{dz}{v(1 - \mathcal{M})} = \tau_{\text{adv}} + \tau_- \sim \frac{H}{v_j(1 - \mathcal{M}_j)}, \quad (57)$$

$$\int_{z_{\text{sh}}}^{z_\nabla} \omega_{\text{buoy}}(z, k_x) \frac{dz}{v} \sim \frac{Hk_x}{(H^2 k_x^2 + \zeta^2)^{\frac{1}{2}}} \omega_{\text{buoy}}(z_i) \tau_{\text{adv}}. \quad (58)$$

The growth rate ω_i can be rewritten as follows:

$$\begin{aligned} \omega_i \sim & \left(1 - \frac{\tau_-}{\tau_Q} \right) \frac{Hk_x}{(H^2 k_x^2 + \zeta^2)^{\frac{1}{2}}} \omega_{\text{buoy}}(z_i) - k_x v_j (1 - \mathcal{M}_j) \\ & + \frac{1}{\tau_Q} \log Q_\nabla Q_{\text{sh}}. \end{aligned} \quad (59)$$

If the coupling efficiencies are moderate ($Q_\nabla Q_{\text{sh}} \sim 1$), the growth rate is at best comparable to the maximum local convective growth rate $\sim (G/H)^{\frac{1}{2}}$, as observed in Fig. 5. Equation (56) can be used to establish a connection between the stability threshold $\chi_0 \sim 3$ and the wavenumber $(k_x H)_0 \sim 3$ of the neutral mode:

$$\chi_0 \sim (k_x H)_0 - \log Q_\nabla Q_{\text{sh}}. \quad (60)$$

This relation can be considered as a consistency check, *a posteriori*, that the product $Q_\nabla Q_{\text{sh}}$ is indeed of order unity.

5.4. Comparison with the hole tone instability of the whistling kettle

The advective-acoustic instabilities studied by FT00, F01, F02, or the rumble instability of ramjets (Abouseif, Keklak & Toong 1984) have in common that the phase of advection is passive. By contrast, vorticity perturbations in the neutrino-driven convection grow exponentially through the Rayleigh-Taylor mechanism during advection from the shock to the gain radius.

A similar active role can be found in the hole tone instability of the whistling kettle (Chanaud & Powell 1965), which relies on the exponential increase of vorticity perturbations during their advection in the shear layer. Note that the hole-tone instability is oscillatory, whereas neutrino-driven convection is purely growing. This can be understood by noting that an oscillation with a frequency ω_r introduces a longitudinal scale $\sim 2\pi v/\omega_r$ in the direction of the flow. The Kelvin-Helmholtz instability involved in the hole tone instability favours a short scale in the direction of the flow, comparable to a few times the transverse size of the shear layer. By contrast, the Rayleigh-Taylor instability involved in neutrino-driven convection favours a long scale in the vertical direction.

5.5. Comparison with the ablative stabilization of the Rayleigh-Taylor instability in accelerated ablative fronts

The stabilization at short wavelength is reminiscent of the “ablative stabilization” of the Rayleigh-Taylor instability observed in laser experiments during the acceleration phase of the ablation front (Bodner 1974). The laser energy is deposited, either directly or indirectly, on the outer region of a spherical shell which is continually ablated. These experiments rely on the inertia of the inner region of the shell to provide confinement for nuclear fusion (see e.g. Lindl 1995). It is instructive to check whether our understanding of the stabilization of convection is compatible with the results obtained in the case of ablative fronts, extensively studied during the last 30 years (see a recent review, including the comparison with flames, by Clavin & Masse 2004). Let us recall that the velocity of the ablation front is set by the thermal diffusion, and is thus very subsonic. It is always unstable with respect to long wavelengths ($k_{\min} = 0$) and always stabilized at short enough wavelength ($k_{\max} < \infty$). The eigenvalue problem for ablation fronts was solved numerically by Takabe et al. (1985), who established the following fitting formula for an effective growth rate:

$$\omega_{\text{eff}} \equiv \alpha (k_x G)^{\frac{1}{2}} - \beta k_x v_a, \quad (61)$$

where v_a is the velocity of the ablation front, G the effective acceleration, $\alpha = 0.9$ and $\beta \sim 3 - 4$. For wavelengths shorter than the size H of the density gradients, the saturation of the Rayleigh-Taylor instability was taken into account in the following global formula (see Eq. (69) in the review by Lindl 1995):

$$\omega_{\text{eff}} \equiv \left(\frac{k_x G}{1 + Hk_x} \right)^{\frac{1}{2}} - \beta k_x v_a. \quad (62)$$

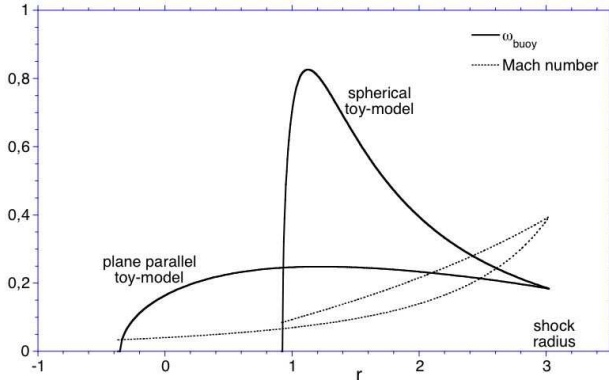


Fig. 9. Two examples of the vertical shape of the local Brunt-Väisälä growth rate $\omega_{\text{buoy}}(r)$ (full line) and Mach number (dotted line), in a plane parallel flow with constant gravity ($\chi = 6.5$) and in a spherical flow ($\chi = 4.1$). Distances are normalized by c_{sh}^2/G and growth rates by G/c_{sh} , where G is the intensity of gravity at the shock radius. Both flows have the same heat flux at the shock. Buoyancy is maximum close to the gain radius in the spherical flow. In both cases, the buoyancy drops abruptly to zero at the gain radius.

The resemblance with Eq. (59) is striking. Much work has been devoted to explaining the stabilizing term $-\beta k_x v_a$ in Eq. (61). The idea of the evanescent pressure feedback is briefly mentioned by Lindl (1995). Goncharov et al. (1996b) stressed the role of thermal diffusion in the stabilization process at short wavelength, despite the absence of an explicit dependence on the diffusion coefficient (see also Clavin & Masse 2004). As a consequence, the stabilization at short wavelength for $\text{Fr} \ll 1$ is such that $k_{\text{max}} \propto \text{Fr}^{-1/3}$ rather than the value $\text{Fr}^{-1/2}$ deduced from a purely kinematic effect. The stabilization effect observed in neutrino-driven convection is thus present in ablative fronts but dominated by an effect of thermal diffusion.

The instability of ablation fronts with respect to long wavelength perturbations $Hk_x \ll 1$ underlines the role of the pressure profile in the vertical direction, which enables an interplay of regions of low entropy gas far upstream of the ablation front, on a large vertical scale, even for large Froude numbers (Goncharov et al. 1996a). These low entropy regions are absent from the problem of neutrino driven convection, because of the presence of the shock.

6. Extrapolation to stalled accretion shocks in spherical geometry

6.1. Tentative extrapolation of the parallel toy model

The equations describing a spherical toy model and its perturbations are written in Appendix F and solved numerically in the next section. The changes introduced in spherical symme-

try appear on the stationary flow equations:

$$\mathcal{L} \equiv \frac{\bar{\mathcal{L}}\rho}{1-\beta} \left[\left(\frac{r_{\text{sh}}}{r} \right)^2 - \beta \left(\frac{T}{T_{\text{sh}}} \right)^6 \right], \quad (63)$$

$$\frac{\partial}{\partial r} (\rho v^2) = 0, \quad (64)$$

$$\frac{\partial}{\partial r} \left(\frac{v^2}{2} + \frac{c^2}{\gamma-1} - \frac{GM}{r} \right) = \frac{c^2}{\gamma} \frac{\partial S}{\partial r}. \quad (65)$$

Neutrino heating, gravity $G \equiv GM/r^2$ and momentum ρv increase inward like r^{-2} . The radial shape of the Brunt-Väisälä frequency $\omega_{\text{buoy}}(r)$ is modified accordingly:

$$\omega_{\text{buoy}} = \frac{GM}{cr_{\text{sh}}^2} \frac{r_{\text{sh}}}{r} \left| \frac{v_{\text{sh}}}{v} \right|^{\frac{1}{2}} \frac{(\alpha\epsilon)^{\frac{1}{2}}}{(1-\beta)^{\frac{1}{2}}} \left[\left(\frac{r_{\text{sh}}}{r} \right)^2 - \beta \left(\frac{T}{T_{\text{sh}}} \right)^6 \right]^{\frac{1}{2}}. \quad (66)$$

The critical heating leading to a postshock reacceleration is decreased by a factor $\alpha \sim 0.5$ due to the convergence of the flow so that ϵ is now defined as

$$\epsilon \equiv -\frac{\gamma-1}{\alpha} \frac{\bar{\mathcal{L}}r_{\text{sh}}^2}{GMv_{\text{sh}}}, \quad (67)$$

$$\alpha \equiv 1 - \frac{2r_{\text{sh}}c_{\text{sh}}^2}{GM}. \quad (68)$$

According to this new definition of ϵ , its estimation for a spherical flow is:

$$\epsilon \sim 0.32 \left(\frac{v_1}{7v_{\text{sh}}} \right) \left(\frac{r_{\text{sh}}}{150\text{km}} \right)^{\frac{1}{2}}. \quad (69)$$

As illustrated on Fig. 9 for $r_{\text{gain}}/r_{\text{sh}} \sim 0.3$, the maximum value of $\omega_{\text{buoy}}(r)$ may be reached close to the gain radius, and may exceed its value at the shock by a large factor. The radial gradients introduced by the spherical geometry may also affect the efficiency Q_V of the vortical-acoustic coupling. As seen in Appendix F, the structure of the perturbed equations (F.5-F.8) is the same as in the parallel toy model (Eqs. (23-26)), the main change consisting in replacing k_x^2 by $l(l+1)/r^2$. A tentative extrapolation to spherical flow of the results obtained in a parallel flow may use a mean radius $(r_{\text{sh}} + r_{\text{gain}})/2$ to translate the horizontal wavenumber k_x into the degree l . Since the most unstable horizontal wavelength is comparable to [1–2] times the vertical size of the gain region in the parallel flow (Fig. 7), the degree l of the most unstable mode should be comparable to

$$l^{\frac{1}{2}}(l+1)^{\frac{1}{2}} \sim [1-2]\pi \left(\frac{r_{\text{sh}}}{H} - \frac{1}{2} \right). \quad (70)$$

Applying in this formula $H/r_{\text{sh}} \sim 0.5$ leads to $l \sim 6$. This correspondence is certainly very crude for low degree modes. Nevertheless, it compares favorably to the results obtained numerically in spherical symmetry in the next section. Fig. 8 further suggests that the mode $l = 1$ would be stabilized by advection unless $\chi > 6$.

6.2. Numerical solution for the eigenmodes in a spherical toy model

The spherical geometry strongly limits the range of parameters $(r_{\text{gain}}/r_{\text{sh}}, \chi)$ that can be reached within reasonable values

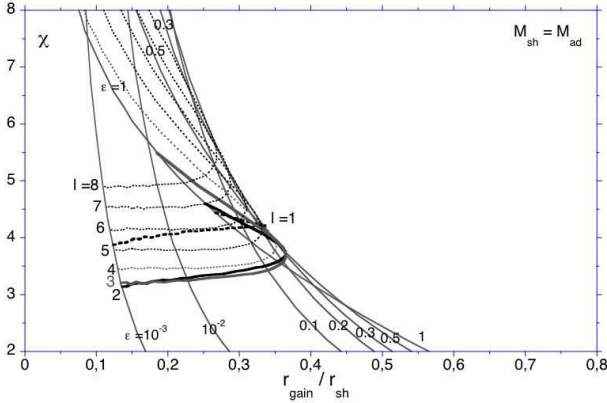


Fig. 10. The thin full lines show the range of (r_{gain}, χ) of the flows with a given value of ϵ , indicated on each line, when the cooling parameter β is varied. Nuclear dissociation is neglected in the upper plot, whereas $M_{sh}/M_{ad} = 0.77$ in the lower plot. The curves labelled by l (thick lines and thin dotted lines) show the stability threshold of a specific low degree perturbation, when the heating parameter ϵ is varied from $\epsilon = 10^{-3}$ to $\epsilon = 1$. The mode $l = 1$ is associated with the thick dashed line. The most unstable modes correspond to $l \sim 2 - 3$ perturbations in flows without dissociation (upper plot), and $l = 4 - 5 - 6$ with dissociation (bottom plot). In both cases, the global stability threshold corresponds to $\chi_0 \sim 3$.

of neutrino heating ($\epsilon \leq 1$). The thin full lines of Fig. 10 show how the parameter space (ϵ, β) defining the flows of our toy-model can be mapped into the plane $(r_{gain}/r_{sh}, \chi)$. This mapping is folded near $\epsilon \sim 0.3$. Note that this folding is also present in the plane parallel toy model, as can be deduced from Figs. 3 and 4. In spherical geometry, high values of χ can only be obtained in flows with a small gain radius. Even with the deceleration due to dissociation (bottom plot of Fig. 10), the flows where $r_{gain}/r_{sh} > 0.6$ have a very moderate parameter $\chi < 4$. The stability analysis of this family of flows is summarized by the thick full lines and thin dotted lines of Fig. 10, obtained as follows: for each heating parameter ϵ in the range $10^{-3} \leq \epsilon \leq 1$, a parameter $\beta(\epsilon, l)$ is determined such that the corresponding

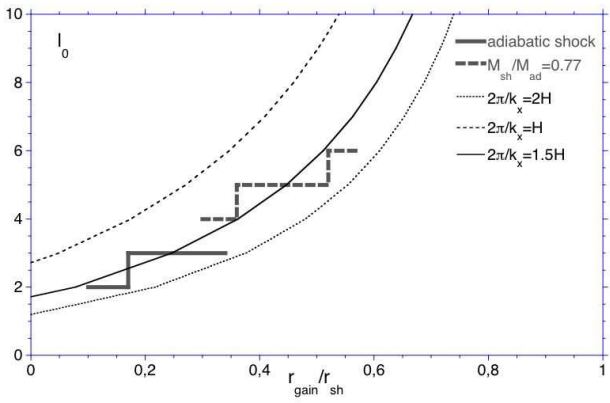


Fig. 11. Degree l of the first unstable mode in the spherical toy model for $\epsilon \leq 0.3$. The thick lines are deduced from Fig. 10 and correspond to a spherical gain region with an adiabatic shock (full line) and with dissociation (dashed line). The thin lines correspond to Eq. (70) extrapolated from the parallel toy model, with $2\pi/k_x = H$ (dashed line), $2\pi/k_x = 1.5H$ (full line) and $2\pi/k_x = 2H$ (dotted line).

flow is marginally stable with respect to perturbations of degree l . The value of the gain radius and χ of this flow is then plotted.

- In both plots, the threshold for convective instability corresponds to $\chi_0 \sim 3$, as in plane parallel flows.

- The degree l of the first unstable mode, plotted in Fig. (11) is surprisingly close to the rough estimate extrapolated from the parallel toy model (Eq. (70)) for $\epsilon \leq 0.3$.

- The destabilization of the mode $l = 1$ is slightly easier than anticipated by the plane parallel toy model. The threshold χ_0^1 for this mode is in the range [4, 6], whereas Fig. 8 would suggest $\chi_0^1 \sim 6 \pm 1$. Moreover, dissociation surprisingly increases the $l = 1$ threshold in a spherical flow, while it would be slightly decreased according to Fig. 8.

6.3. Effect of acoustic reflection below the gain radius

In the above analysis, the convective instability generates a pressure perturbation which is evanescent below the gain region. In the parallel toy model,

$$\frac{\delta p}{p} \propto \exp \left[-k_x(1 - M^2)z \right]. \quad (71)$$

A reflective boundary at a distance $\Delta z_{ac} > H$ from the shock may play a role on the convective instability only if the amplitude of the reflected pressure perturbation is significant:

$$k_x < \frac{1}{\Delta z_{ac}}. \quad (72)$$

With $k_x \sim \pi/H$ according to Fig. 7, the most unstable mode should be hardly affected by a possible reflection of acoustic waves:

$$\exp \left(-\pi \frac{\Delta z_{ac}}{H} \right) \ll 1. \quad (73)$$

According to Eq. (71), the influence of acoustic reflection is strongest for the modes such that $k_x \Delta z_{\text{ac}} \ll 1$, i.e. low degree modes. In a subsonic flow, the vortical-acoustic coupling produces comparable amounts of acoustic power in the upward and downward directions. An efficient acoustic reflection below the gain radius may increase the efficiency Q of the vortical-acoustic cycle by a factor 2 at most. This effect is thus bound to be marginal.

6.4. Effect of the advective-acoustic coupling below the gain radius

The coupling between advected and acoustic perturbations below the gain radius may play an important role in determining the global stability of the flow. Strong gradients are produced in the flow below the gain radius:

- (i) on a large scale, by the convergence of the flow and the gravitational potential,
- (ii) on a smaller scale, by the strong cooling close to the surface of the neutron star.

A global advective-acoustic cycle may be unstable between the shock and the neutron star, even in the absence of a heated region (Galletti & Foglizzo, in preparation).

Our understanding of the convective instability in an advected flow involves a pressure feedback due to the flow gradients within the gain region. This leads us to expect a possible co-operation between the convective instability and the global advective-acoustic cycle on a larger vertical scale than the size of the gain region. The most unstable mode might correspond to a global cycle in which vorticity perturbations are amplified during their advection through the gain region, advected below the gain radius and efficiently coupled to pressure in the region of cooling, where the acoustic feedback propagates upwards towards the shock. In numerical simulations, the possibility of such global cycles stresses the important roles of both the spatial resolution well below the gain radius, and the lower boundary conditions.

7. Conclusions

A toy model has been developed and studied in depth in order to understand the effect of advection on the linear growth of the convective instability in the gain region immediately below a stationary shock. New results have been obtained through a numerical calculation of the eigenmodes, explained by a vortical-acoustic cycle, and extrapolated to core-collapse flows.

(i) The numerical solution of the boundary value problem reveals that convection can be significantly stabilized by advection. The existence of a negative entropy gradient is not a sufficient condition for the convective instability in an advected flow. Not only the growth rate of the fastest growing mode is diminished, but also the range of unstable wavelengths is modified.

- The effect of advection on the convective instability is essentially governed by a single dimensionless parameter χ , defined by Eq. (40), which compares the buoyant and the advective

timescales. The value of χ can be directly measured in numerical simulations.

- As illustrated on Fig. 5, a convective mode may develop in the gain region, with a linear growth rate significantly slower than the local convective growth rate if the value of χ is moderate ($3 < \chi < 5$). In the plane parallel flow of our toy model, the gain region is linearly stable if $\chi < 3$.

- The minimum and maximum unstable wave numbers are directly related to χ according to $Hk_{\min} \propto 1/\chi$, $Hk_{\max} \propto \chi$ as shown on Fig. 8.

- The horizontal wavelength of the first unstable mode when $\chi \sim 3$ is comparable to twice the vertical size of the gain region.

(ii) The stabilisation by advection and the scalings of k_{\min} , k_{\max} are understood in terms of a vortical-acoustic cycle within the gain region. This interpretation does not require the explicit calculation of the coupling coefficients Q_{sh} and Q_{v} , whose product is assumed to be of order unity in the low frequency limit. This instability is purely growing, without oscillations.

- The unstable cycle is fed by the phase of advection, which plays an active role through the local Rayleigh-Taylor instability. In this sense a parallel can be drawn with the hole tone instability of the whistling kettle (Chanaud & Powell 1965).

- The scaling $Hk_{\max} \propto \chi$ is a consequence of the evanescent pressure feedback of small scale perturbations. It is related to the “ablative stabilization” of short wavelengths in accelerated ablation fronts (Lindl 1995).

- The scaling $Hk_{\min} \propto 1/\chi$ for long horizontal wavelengths is a consequence of the vicinity of the shock. Proving this point required an estimate of the Rayleigh-Taylor growth rate in a density gradient close to a wall or a free surface (Appendix E).

- The assumption that $|Q_{\text{sh}}Q_{\text{v}}|$ is of order unity is consistent with the fact that the stability threshold χ_0 is comparable to the horizontal wavenumber of the first unstable mode $(k_x H)_0 \sim 3$ (Eq. (60)).

(iii) These results can be used as a guide to better understand the convective motions behind a stalled accretion shock in core collapse supernovae, and in particular their contribution to an $l = 1$ asymmetry. The parameter χ can be measured directly in numerical simulations. A rough estimate, in Eq. (5), suggests that χ may be close to the threshold of stabilisation. The stabilization of long wavelength perturbations, illustrated by Fig. 5 and Fig. 8, can be a severe impediment to the development of a residual $l = 1$ mode. The solution of the eigenvalue problem in a spherical toy model confirms the threshold $\chi_0 \sim 3$ for the convective instability, and shows examples where the mode $l = 1$ is stable unless $\chi > 4 - 6$. Convective motions associated to a small value of $\chi \leq 3$ may be a hint that the result of the simulation is not the consequence of the gain region alone, but depends significantly on an acoustic feedback occurring below the gain radius. In such case, particular attention should be paid to the grid size below the gain region, in order to treat correctly the advective-acoustic coupling. The steep density gradient at the proto-neutron star surface may have also some influence through acoustic reflexion.

In this sense, these results do not preclude the possible destabilization of the $l = 1$ mode due to coupling processes occurring below the gain radius. The entropy gradients in the gain region may even contribute to enhance the efficiency Q of a global vortical-acoustic cycle by a factor of the order of $\exp\chi$. The study of such global cycles is the subject of forthcoming papers which consider a linear analysis (Foglizzo et al., in preparation) as well as numerical simulations of the nonlinear growth of nonspherical modes in the supernova core (Scheck et al., in preparation).

Acknowledgements. TF thanks Pascal Galletti for stimulating discussions. The authors are grateful for funding by Egide (France) and by DAAD (Germany) through their “Procope” exchange program. Support by the Sonderforschungsbereich 375 on “Astro-Particle Physics” of the Deutsche Forschungsgemeinschaft is acknowledged.

Appendix A: Photodissociation at the shock

The energy cost of dissociation is $\mathcal{E} \sim 8.8\text{MeV}$ per nucleon for iron. This energy is assumed to be lost immediately after the shock:

$$\frac{v_1^2}{2} + \frac{c_1^2}{\gamma-1} = \frac{v_{\text{sh}}^2}{2} + \frac{c_{\text{sh}}^2}{\gamma-1} + \mathcal{E}, \quad (\text{A.1})$$

The effect of dissociation can be parametrized by the value of the postshock Mach number $\mathcal{M}_{\text{sh}} \leq \mathcal{M}_{\text{ad}}$, according to:

$$\frac{\mathcal{E}}{\frac{v_1^2}{2} + \frac{c_1^2}{\gamma-1}} = \left(1 - \frac{\mathcal{M}_{\text{sh}}^2}{\mathcal{M}_{\text{ad}}^2}\right) \left(1 - \frac{\mathcal{M}_{\text{sh}}^2}{\mathcal{M}_1^2}\right), \quad (\text{A.2})$$

$$\frac{v_{\text{sh}}}{v_1} = \frac{\mathcal{M}_{\text{sh}}^2}{\mathcal{M}_1^2} \frac{1 + \gamma \mathcal{M}_1^2}{1 + \gamma \mathcal{M}_{\text{sh}}^2}, \quad (\text{A.3})$$

$$\frac{c_{\text{sh}}}{c_1} = \frac{\mathcal{M}_{\text{sh}}}{\mathcal{M}_1} \frac{1 + \gamma \mathcal{M}_1^2}{1 + \gamma \mathcal{M}_{\text{sh}}^2}, \quad (\text{A.4})$$

where the Mach number is defined by $\mathcal{M} \equiv |v|/c > 0$. According to Eqs. (A.3) and (A.4), $v_1/v_{\text{sh}} = \gamma \mathcal{M}_1^2$ and $c_{\text{sh}} = c_1$ if $\mathcal{M}_{\text{sh}} \mathcal{M}_1 = 1/\gamma$. This rather extreme case is referred to as the “isenthalpic shock”.

Appendix B: Linearized equations

The heating function described by Eq. (9) is perturbed as follows:

$$\delta\left(\frac{\mathcal{L}}{\rho v}\right) = -\nabla S \frac{c^2}{\gamma} \frac{\delta v}{v} - \frac{6\beta \nabla S_{\text{sh}}}{\gamma(1-\beta)} \frac{v_{\text{sh}}}{v} c_{\text{sh}}^2 \left(\frac{c}{c_{\text{sh}}}\right)^{12} \frac{\delta c^2}{c^2}, \quad (\text{B.1})$$

$$\delta\left(\frac{\mathcal{L}}{\rho v}\right) = \frac{\gamma}{c^2} \delta\left(\frac{\mathcal{L}}{\rho v}\right) - \frac{\delta c^2}{c^2} \nabla S, \quad (\text{B.2})$$

with

$$\frac{\delta v}{v} = \frac{1}{1-\mathcal{M}^2} \left(h - \frac{f}{c^2} + \delta S \right), \quad (\text{B.3})$$

$$\frac{\delta c^2}{c^2} = \frac{\gamma-1}{1-\mathcal{M}^2} \left(\frac{f}{c^2} - \mathcal{M}^2 h - \mathcal{M}^2 \delta S \right). \quad (\text{B.4})$$

Appendix C: Lower boundary condition

In an adiabatic, uniform flow, the perturbation f_S associated with an advected entropy perturbation δS such that $\delta K = 0$, and the perturbation f_K associated to δK with $\delta S = 0$ are respectively given by:

$$f_S = \frac{1 - \mathcal{M}^2}{1 - \mu^2 \mathcal{M}^2} c^2 \frac{\delta S}{\gamma}, \quad (\text{C.1})$$

$$f_K = \frac{\mathcal{M}^2(1 - \mu^2)}{1 - \mu^2 \mathcal{M}^2} \frac{\delta K}{k_x^2}. \quad (\text{C.2})$$

Both are associated with the same wave number k_z^0 of advected perturbations:

$$k_z^0 = \frac{\omega}{v}. \quad (\text{C.3})$$

Pressure perturbations f_{\pm} correspond to the solution of the differential system (23) to (26) with $\mathcal{L} = 0$, $\delta S = 0$ and $\delta K = 0$. The longitudinal wavenumber k^{\pm} of acoustic perturbations is equal to

$$k^{\pm} \equiv \frac{\omega}{c} \frac{\mathcal{M} \mp \mu}{1 - \mathcal{M}^2}, \quad (\text{C.4})$$

where the sign of μ is defined such that $\text{Im}(k^+) < 0$ when $\text{Real}(\mu^2) < 0$ (evanescent wave), and $\text{Real}(k^+) < 0$ when $\text{Real}(\mu^2) > 0$ (downward propagation). The components f^{\pm} are deduced from the values of f , h and Eqs. (C.1)–(C.2):

$$f^{\pm} = \frac{1}{2} f \pm \frac{\mathcal{M} c^2}{2\mu} (h + \delta S) - \frac{1 \pm \mu \mathcal{M}}{2} \left(f^S \pm \frac{f_K}{\mu \mathcal{M}} \right), \quad (\text{C.5})$$

$$h^{\pm} = \pm \frac{\mu}{\mathcal{M}} \frac{f^{\pm}}{c^2}. \quad (\text{C.6})$$

Appendix D: Neutral mode $\omega = 0$

The linearized equations for $\omega = 0$ are simplest when using f , h , δS , v_x . The Euler equation in the transverse direction and the definition of δK lead to:

$$v \delta w_y = i k_x \frac{c^2}{\gamma} \delta S - i k_x f, \quad (\text{D.1})$$

$$\delta K = k_x^2 f. \quad (\text{D.2})$$

The differential system is thus:

$$\frac{\partial f}{\partial z} = \delta \left(\frac{\mathcal{L}}{\rho v} \right), \quad (\text{D.3})$$

$$\frac{\partial h}{\partial z} = - \frac{i k_x \delta v_x}{v}, \quad (\text{D.4})$$

$$\frac{\partial \delta S}{\partial z} = \delta \left(\frac{\mathcal{L}}{\rho v} \right), \quad (\text{D.5})$$

$$\frac{\partial \delta v_x}{\partial z} = \frac{-i k_x}{v(1-\mathcal{M}^2)} \left\{ f - v^2 h - \frac{c^2}{\gamma} [1 + (\gamma-1)\mathcal{M}^2] \delta S \right\}. \quad (\text{D.6})$$

On the shock surface, the boundary conditions are measured for a shock displacement $\Delta\zeta$:

$$f_{\text{sh}} = -\Delta\zeta \frac{c_{\text{sh}}^2}{\gamma} \nabla S, \quad (\text{D.7})$$

$$h_{\text{sh}} = 0, \quad (\text{D.8})$$

$$\delta S_{\text{sh}} = -\Delta\zeta \left[\nabla S + \left(1 - \frac{v_{\text{sh}}}{v_1} \right) \frac{\gamma}{c_{\text{sh}}^2} \nabla \phi \right], \quad (\text{D.9})$$

$$(ik_x \delta v_x)_{\text{sh}} = -k_x^2 (v_1 - v_{\text{sh}}) \Delta \zeta. \quad (\text{D.10})$$

The lower boundary condition in the adiabatic part of the flow ($\nabla S = 0$) is determined by remarking that

$$\frac{\partial^2 \delta v_x}{\partial z^2} - \frac{k_x^2 \delta v_x}{1 - \mathcal{M}^2} = 0. \quad (\text{D.11})$$

The evanescent solution when $z \rightarrow -\infty$ is selected by imposing:

$$\frac{\partial \delta v_x}{\partial z} - \frac{k_x \delta v_x}{(1 - \mathcal{M}^2)^{\frac{1}{2}}} = 0. \quad (\text{D.12})$$

The continuity of $f, h, \delta S, k_x v_x$ at the lower boundary implies the continuity of $\partial \delta v_x / \partial z$ according to Eq. (D.6). The boundary condition (D.12) is thus continuous across the gain radius (only f and δS have discontinuous derivatives across the gain radius).

Appendix E: Rayleigh-Taylor instability in a density gradient close to a wall or a free surface

Let us consider a density profile $\rho(z)$ in a uniform gravity G . A layer of finite thickness Δz with a density gradient $\rho \propto \exp(+z/H)$ stands on top of a fluid with uniform density. For simplicity, the gas is assumed to be incompressible ($\nabla \cdot v = 0$). The effect of the upper boundary condition z_{up} is tested by considering two cases. The gas is either bounded by a rigid wall ($\delta v_z(z_{\text{up}}) = 0$) or by a free surface ($\delta p(z_{\text{up}}) = 0$). The linearized perturbations in the plane (x, z) satisfy the following system of equations:

$$\frac{\partial \delta v_z}{\partial z} + ik_x \delta v_x = 0, \quad (\text{E.1})$$

$$-i\omega \delta \rho + \delta v_z \frac{\partial \rho}{\partial z} = 0, \quad (\text{E.2})$$

$$-i\omega \delta v_z + \frac{1}{\rho} \frac{\partial \delta p}{\partial z} - \frac{\delta p}{\rho} g = 0, \quad (\text{E.3})$$

$$-i\omega \delta v_x + ik_x \frac{\delta p}{\rho} = 0. \quad (\text{E.4})$$

The differential equation satisfied by the perturbed velocity δv_z is

$$\frac{\partial^2}{\partial z^2} \delta v_z + \frac{\partial \log \rho}{\partial z} \frac{\partial \delta v_z}{\partial z} - k_x^2 \left[1 + \frac{G}{\omega^2} \frac{\partial \log \rho}{\partial z} \right] = 0. \quad (\text{E.5})$$

Let us consider the following density profile:

$$\rho = \rho_0 e^{+z/H} \text{ for } 0 < z < z_{\text{up}}, \quad (\text{E.6})$$

$$\rho = \rho_0 \text{ for } z < 0. \quad (\text{E.7})$$

The general solution is described by:

$$\delta v_z \propto \alpha_+ e^{\lambda^+ z} + \alpha_- e^{\lambda^- z} \text{ for } 0 < z < z_{\text{up}}, \quad (\text{E.8})$$

$$\delta v_z \propto \beta_+ e^{+kz} + \beta_- e^{-kz} \text{ for } z < 0, \quad (\text{E.9})$$

where λ^\pm is defined by

$$\lambda^\pm = \frac{1}{2} \left(-\frac{1}{H} \pm i \Delta^{\frac{1}{2}} \right), \quad (\text{E.10})$$

$$\Delta = \frac{4k_x^2 G}{(-\omega^2)H} - \left[4k_x^2 + \frac{1}{H^2} \right]. \quad (\text{E.11})$$

The constants α_\pm and β_\pm are determined by specifying the upper boundary condition, the continuity of velocity and pressure at $z = 0$, and the decay of perturbations when $z \rightarrow -\infty$. These boundary conditions translate into the following dispersion relation:

$$\Delta > 0, \quad (\text{E.12})$$

$$\tan \frac{\Delta^{\frac{1}{2}} z_{\text{up}}}{2} = -\frac{H \Delta^{\frac{1}{2}}}{1 + 2Hk_x} \text{ if } \delta v_z(z_{\text{up}}) = 0, \quad (\text{E.13})$$

$$\tan \frac{\Delta^{\frac{1}{2}} z_{\text{up}}}{2} = \frac{2k_x H^2 \Delta^{\frac{1}{2}}}{1 + 2Hk_x + H^2 \Delta} \text{ if } \delta p(z_{\text{up}}) = 0. \quad (\text{E.14})$$

Remarking that a solution of Eq. (E.13) (resp. Eq. (E.14)) stands in the interval $\pi < \Delta^{\frac{1}{2}} z_{\text{up}} < 2\pi$ (resp. $2\pi < \Delta^{\frac{1}{2}} z_{\text{up}} < 3\pi$), a number $\zeta(k_x)$ must exist such that the highest growth rate $\omega_i(k_x)$ is

$$\omega_i(k_x) = \frac{Hk_x}{(H^2 k_x^2 + \zeta^2)^{\frac{1}{2}}} \left(\frac{G}{H} \right)^{\frac{1}{2}}, \quad (\text{E.15})$$

$$\zeta \equiv \left(\frac{1}{4} + \frac{\eta^2 \pi^2 H^2}{4 z_{\text{up}}^2} \right)^{\frac{1}{2}} \quad (\text{E.16})$$

$$1 < \eta < 2 \text{ if } \delta v_z(z_{\text{up}}) = 0, \quad (\text{E.17})$$

$$2 < \eta < 3 \text{ if } \delta p(z_{\text{up}}) = 0. \quad (\text{E.18})$$

Note that another solution of Eq. (E.14), with $0 < \eta < 1$, exists if $z_{\text{up}}/H < 2$, for

$$Hk_x > \frac{1}{2} \frac{z_{\text{up}}}{z_{\text{up}} + 2H}. \quad (\text{E.19})$$

In the short wavelength limit $k_x \gg 1/z_{\text{up}}$ and $k_x \gg 1/H$, the growth rate $\omega_i \sim (G/H)^{\frac{1}{2}}$ is recovered, independently of the boundary condition. The growth rate for very long wavelengths $Hk_x < z_{\text{up}}/8H$ is thus always slightly larger for a wall than for a free boundary. The free boundary is more favourable than a wall to the growth of perturbations whose wavelengths satisfies Eq. (E.19), if $z_{\text{up}}/H < 2$.

In any case, the growth rate is always proportionnal to the wavenumber in the long wavelength limit:

$$\omega_i(k_x) \sim \frac{Hk_x}{\zeta} \left(\frac{G}{H} \right)^{\frac{1}{2}}. \quad (\text{E.20})$$

If $z_{\text{up}} \sim H$, the parameter ζ is broadly contained in the interval $[1/2, 5]$, depending on the boundary conditions.

Appendix F: Spherical flow

F.1. Mach number gradient and change of pressure gradient across the shock

The radial derivative of the Mach number in our toy model is deduced from Eqs. (12), (13) and (14):

$$\frac{1}{\mathcal{M}} \frac{\partial \mathcal{M}}{\partial r} = \frac{1}{1 - \mathcal{M}^2} \left[\frac{\gamma + 1}{2c^2} \frac{GM}{r^2} - \frac{2 + (\gamma - 1)\mathcal{M}^2}{r} \right]$$

$$+ \frac{\gamma-1}{\gamma} (1 + \gamma \mathcal{M}^2) \frac{\nabla S}{2} \Big]. \quad (\text{F.1})$$

This quantity is negative at the shock if the heating is strong enough. The threshold $(d\mathcal{M}/dr)_{sh} = 0$, expressed in our dimensionless units corresponds to:

$$\epsilon = \frac{1}{\alpha(1 + \gamma \mathcal{M}_{sh}^2)} \{ \gamma + 1 - (1 - \alpha) [2 + (\gamma - 1) \mathcal{M}_{sh}^2] \} > 1. \quad (\text{F.2})$$

In our toy model, $\epsilon = 1$ corresponds to $(dv/dr)_{sh} = 0$. Since $(dc/dr)_{sh} < 0$ in the gain region near the shock, this implies that $(d\mathcal{M}/dr)_{sh} > 0$ even for $\epsilon = 1$. Changing the sign of $(d\mathcal{M}/dr)_{sh}$ requires an even higher value of ϵ , above unity.

The instability argument of Nobuta & Hanawa (1994) refers to the change of the gradient of the total pressure $P + \rho v^2$ across the shock. In a spherical flow, this change can be deduced from the radial Euler equation, as follows:

$$\left[\frac{\partial}{\partial r} (P + \rho v^2) \right]_1 - \left[\frac{\partial}{\partial r} (P + \rho v^2) \right]_{sh} = (\rho_{sh} - \rho_1) \frac{GM}{r_{sh}^2} \left[1 - \frac{4}{7} \left(\frac{v_1^2 r_{sh}}{2GM} \right) \left(\frac{7v_{sh}}{v_1} \right) \right] > 0. \quad (\text{F.3})$$

Going outward, the jump at the shock is always positive if the incoming gas is approximately in free fall and if the shock is strong enough. Actually the infall velocity of the gas ahead of the shock must be expected to be somewhat lower than free-fall because of non-vanishing pressure effects. The sign of Eq. (F.3) was negative in F02 because the supersonic gas was artificially thrown at a velocity higher than free fall, for the sake of obtaining a stationary solution with a shock. In the calculation of Nakayama (1992), this sign was also negative due to the contribution of angular momentum.

F.2. Gain region

The definition of δK is the same as in Eq. (5) of F01:

$$\delta K \equiv r^2 v \cdot \nabla \times \delta w + \frac{l(l+1)c^2}{\gamma} \delta S. \quad (\text{F.4})$$

If $\omega \neq 0$, the perturbed equations are as follows:

$$\frac{\partial f}{\partial r} = \frac{i\omega v}{1 - \mathcal{M}^2} \left\{ h - \frac{f}{c^2} + \left[\gamma - 1 + \frac{1}{\mathcal{M}^2} \right] \frac{\delta S}{\gamma} \right\} + \delta \left(\frac{\mathcal{L}}{\rho v} \right), \quad (\text{F.5})$$

$$\frac{\partial h}{\partial r} = \frac{i\omega}{v(1 - \mathcal{M}^2)} \left\{ \frac{\mu^2}{c^2} f - \mathcal{M}^2 h - \delta S \right\} + \frac{i\delta K}{\omega r^2 v}, \quad (\text{F.6})$$

$$\frac{\partial \delta S}{\partial r} = \frac{i\omega}{v} \delta S + \delta \left(\frac{\mathcal{L}}{\rho v} \right), \quad (\text{F.7})$$

$$\frac{\partial \delta K}{\partial r} = \frac{i\omega}{v} \delta K + l(l+1) \delta \left(\frac{\mathcal{L}}{\rho v} \right), \quad (\text{F.8})$$

$$\mu^2 \equiv 1 - \frac{l(l+1)c^2}{\omega^2 r^2} (1 - \mathcal{M}^2). \quad (\text{F.9})$$

F.3. Boundary condition in the spherical toy model

The boundary conditions for δS_{sh} and δK_{sh} include the following spherical corrections:

$$\frac{\delta S_{sh}}{\gamma} = -\Delta\zeta \left[\frac{\nabla S}{\gamma} + \left(1 - \frac{v_{sh}}{v_1} \right) \frac{GM}{r_{sh}^2 c_{sh}^2} \left(1 - 4 \frac{v_{sh}}{v_1} \frac{r_{sh} v_1^2}{2GM} \right) \right]$$

$$- \frac{v_1 \Delta v}{c^2} \left(1 - \frac{v_{sh}}{v_1} \right)^2, \quad (\text{F.10})$$

$$\delta K_{sh} = -l(l+1) \Delta\zeta \frac{c^2}{\gamma} \nabla S, \quad (\text{F.11})$$

The leaking boundary condition becomes:

$$\frac{\mu}{\mathcal{M}} \frac{f}{c^2} - h - \left(\gamma + \frac{\mu}{\mathcal{M}} \frac{1 - \mathcal{M}^2}{1 + \mu\mathcal{M}} \right) \frac{\delta S}{\gamma} + \frac{1 - \mu^2}{1 + \mu\mathcal{M}} \frac{\delta K}{l(l+1)c^2} = 0. \quad (\text{F.12})$$

F.4. Neutral mode $\omega = 0$ in a spherical flow

In a spherical flow, $ik_x v_x$ is replaced by the quantity δA associated to the divergence of the transverse velocity perturbation:

$$\delta A \equiv \frac{r}{\sin\theta} \left[\frac{\partial}{\partial\theta} (\sin\theta \delta v_\theta) + \frac{\partial \delta v_\varphi}{\partial\varphi} \right]. \quad (\text{F.13})$$

The Euler equation in the transverse directions and the definition of δK lead to:

$$v \delta w_\varphi = \frac{c^2}{\gamma r} \frac{\partial \delta S}{\partial\theta} - \frac{1}{r} \frac{\partial f}{\partial\theta}, \quad (\text{F.14})$$

$$v \delta w_\theta = -\frac{c^2}{\gamma r \sin\theta} \frac{\partial \delta S}{\partial\varphi} + \frac{1}{r \sin\theta} \frac{\partial f}{\partial\varphi}, \quad (\text{F.15})$$

$$\delta K = l(l+1)f. \quad (\text{F.16})$$

The differential system is as follows:

$$\frac{\partial f}{\partial r} = \delta \left(\frac{\mathcal{L}}{\rho v} \right), \quad (\text{F.17})$$

$$\frac{\partial h}{\partial r} = -\frac{\delta A}{r^2 v}, \quad (\text{F.18})$$

$$\frac{\partial \delta S}{\partial r} = \delta \left(\frac{\mathcal{L}}{\rho v} \right), \quad (\text{F.19})$$

$$\frac{\partial \delta A}{\partial r} = \frac{l(l+1)}{v(1 - \mathcal{M}^2)} \left\{ f - v^2 h - \frac{c^2}{\gamma} [1 + (\gamma - 1) \mathcal{M}^2] \delta S \right\}. \quad (\text{F.20})$$

The spherical corrections for the boundary conditions are:

$$f_{sh} = -\Delta\zeta \frac{c_{sh}^2}{\gamma} \nabla S, \quad (\text{F.21})$$

$$h_{sh} = 0, \quad (\text{F.22})$$

$$\delta S_{sh} = -\Delta\zeta \left[\nabla S + \left(1 - \frac{v_{sh}}{v_1} \right) \frac{GM}{r_{sh}^2 c_{sh}^2} \left(1 - 4 \frac{v_{sh}}{v_1} \frac{r_{sh} v_1^2}{2GM} \right) \right], \quad (\text{F.23})$$

$$\delta A_{sh} = -l(l+1)(v_1 - v_{sh}) \Delta\zeta. \quad (\text{F.24})$$

The lower boundary condition is determined by choosing the evanescent solution when the flow gradients are neglected

$$\frac{\partial \delta A}{\partial r} - \frac{l^{\frac{1}{2}}(l+1)^{\frac{1}{2}}}{r} \frac{\delta A}{1 - \mathcal{M}^2} = 0. \quad (\text{F.25})$$

References

Abouseif, G.E., Keklak, J.A., Toong, T.Y. 1984, Combustion Science and Technology 36, 83

Arnett, W.D. 1987, IAU Symp. 125, The Origin and Evolution of Neutron Stars, ed. D.J. Helfand & J.-H. Huang (Dordrecht: Reidel), 273

Bethe, H.A. 1990, Rev. Mod. Phys. 62, 801

Bethe, H.A. 1993, ApJ 412, 192

Bethe, H.A., Brown, G.E., Cooperstein, J. 1987, ApJ 322, 201

Bethe, H.A., Wilson, J.R. 1985, ApJ 295, 14

Blondin, J.M., Mezzacappa, A., DeMarino, C. 2003, ApJ 584, 971

Bodner, S.E. 1974, Phys. Rev. Lett. 33, 761

Burrows, A. 1987, ApJ 318, L57

Burrows, A., Goshy, J. 1993, ApJ 416, L75

Burrows, A., Hayes, J., Fryxell, B.A. 1995, ApJ 450, 830

Chanaud R.C., Powell A. 1965, J. Acoust. Soc. Am. 37, 902

Chandrasekhar, S. 1961, "Hydrodynamic and hydromagnetic stability", Dover Publication Inc.

Clavin, P., Masse, L. 2004, Phys. Plasm. 11, 690

Foglizzo, T. 2001, A&A 368, 311 (F01)

Foglizzo, T. 2002, A&A 392, 353 (F02)

Foglizzo, T., Galletti, P., Ruffert, M. 2005, A&A 435, 397 (FGR05)

Foglizzo, T., Tagger, M. 2000, A&A 363, 174 (FT00)

Goncharov, V.N., Betti, R., McCrory, R.L., Sorotokin, P., Verdon, C.P. 1996a, Phys. Plasm. 3, 1402

Goncharov, V.N., Betti, R., McCrory, R.L., Verdon, C.P. 1996b, Phys. Plasm. 3, 4665

Herant, M. 1995, Phys. Rep. 256, 117

Herant, M., Benz, W., Colgate, S. 1992, ApJ 395, 642

Herant, M., Benz, W., Hix, W.R., Fryer, C.L., Colgate, S.A. 1994, ApJ 435, 339

Janka, H.-T. 2001, A&A 368, 527

Janka, H.-T., Müller, E. 1996, A&A 306, 167

Janka, H.-T., Müller, E. 1995, ApJ 448, L109

Landau, L., Lifschitz, E. 1989, Fluid Mechanics, Editions MIR

Lindl, J. 1995, Phys. Plasm. 2, 3933

Mezzacappa, A., et al. 1998, ApJ 495, 911

Nakayama, K. 1992, MNRAS 259, 259

Nobuta, K., Hanawa, T. 1994, PASJ 46, 257

Scheck, L., Plewa, T., Janka, H.-T., Müller, E. 2004, Phys. Rev. Lett. 92, 1

Takabe, H., Mima, K., Montierth, L., Morse, R.L. 1985, Phys. Fluids 28, 3676

Thompson, C. 2000, ApJ 534, 915

Woosley, S.E. 1987, IAU Symp. 125, The Origin and Evolution of Neutron Stars, ed. D.J. Helfand & J.-H. Huang (Dordrecht: Reidel), 255

Yamasaki, T., Yamada, S. 2005, ApJ 623, 1000